The 2013 World Congress on
Advances in Structural Engineering and Mechanics (ASEM13)
Jeju, Korea, September 8-12, 2013

Keynote Paper

Hydration Heat and Thermal Stress in Concrete Structures

*Jin-Keun Kim[1)] and Sang-Lyul Cha[2)]

Department of Civil and Environmental Engineering, KAIST, Daejeon 305-600, Korea
[1)] concrete1@kaist.ac.kr

ABSTRACT

Thermal stress induced by hydration heat should be predicted to control the cracks of structures at early age. In this paper, included, that is, two subjects are 1) Development of numerical simulation for predicting temperature distribution and thermal stress in concrete structures, 2) Development of a device for measuring thermal stress. Several related subjects are also presented. Although two approaches predicted thermal stress successfully, further research needs to be performed to predict more accurate thermal stress.

1. INTRODUCTION

During construction of mass concrete structures, thermal stress produced by the hydration heat of cement could occur cracks in concrete structures. Since cracks in concrete structures make problems for durability and serviceability, they should be controlled.

Nowadays, as concrete strength becomes higher and concrete structures become larger, the cracks induced by thermal stress occurs more frequently and is more important. Therefore, it has been increasing demand for controlling cracks induced by thermal stress.

A lot of research work has been done in developing more accurate methods for predicting thermal stress. However, there is still large discrepancy between the thermal stresses in real structures and the results by simulations.

In this paper, several devices and methods related to the hydration heat and thermal stress in concrete are suggested for more accurate prediction of thermal stresses.

2. FINITE ELEMENT METHOD FOR PREDICTION OF THERMAL STRESS

2.1 Properties of concrete

General design process of mass concrete is shown in Fig. 1. As shown in Fig.1, the

[1)] Professor
[2)] Graduate student

largest source of uncertainty mostly comes from the properties of concrete at early age and coefficient of heat transfer. Therefore, much research work has been carried out to obtain properties of concrete and coefficient of heat transfer [2-11].

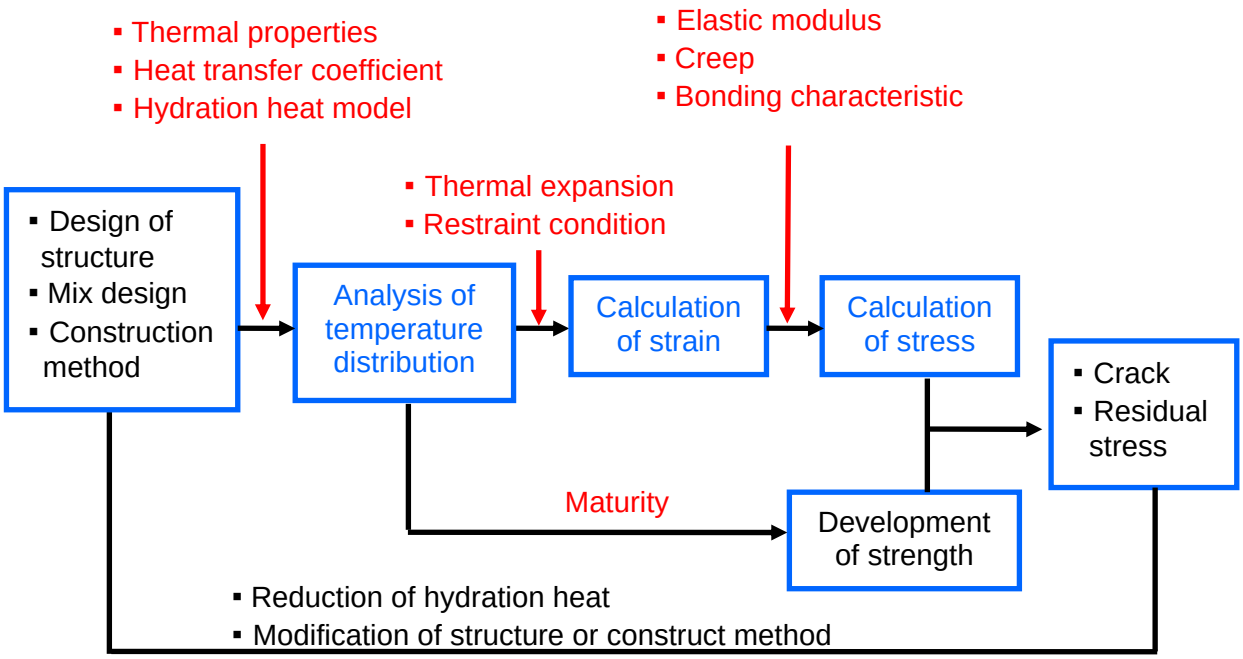

Fig. 1 Design process of mass concrete

2.1.1 Hydration heat

After portland cement is mixed with water, heat is generated by the result of the chemical reaction between cement and water. This heat is called hydration heat. Hydration heat is one of the most important factors because it is used as source of heat in concrete structures.

In general, adiabatic temperature rise test has been used to calculate hydration heat. The result of adiabatic temperature rise test is quite accurate because it measures temperature rise of concrete which is kept on adiabatic condition. However, it is not applicable in construction field because the testing machine is expensive and large.

Therefore, a new equipment for measuring temperature rise of concrete has been developed which is shown in Fig. 2 [1]. This equipment measures semi-adiabatic temperature rise is obtained by this equipment and the heat loss of concrete by the equipment is compensated. Eq. (1) expresses temperature rise of concrete by compensation of heat loss.

$$\Delta T_{adi}(t) = \Delta T(t) + \frac{1}{\rho C V} \int_0^t \int_S h_a (T_s(t) - T_{air}(t)) dA dt \qquad (1)$$

where, $\Delta T_{adi}(t)$ is adiabatic temperature rise at time t (℃), $\Delta T(t)$ is temperature rise at time t (℃), ρ is density of concrete(kg/m^3), C is specific heat of concrete(kcal/kg·℃),

V is volume of concrete(m^3), h_a is convective heat transfer coefficient(kcal/h·m^2·℃), $T_s(t)$ is specimen surface temperature(℃) and $T_{air}(t)$ is ambient temperature(℃).

Fig. 2 Equipment for measuring temperature rise of concrete [1]

The result of the equipment is compared with adiabatic temperature rise test. As shown in Fig. 3, the result is quite similar to the result of adiabatic temperature rise test.

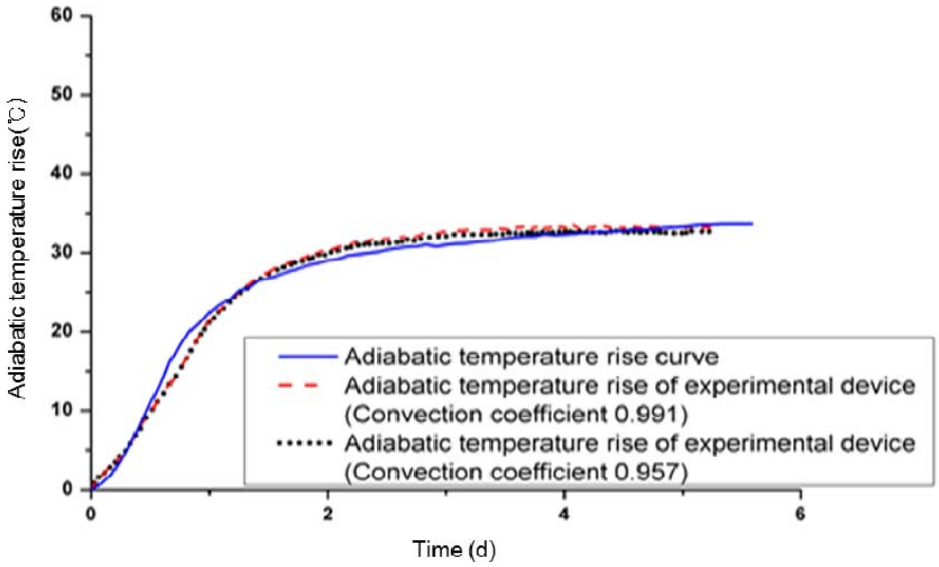

Fig. 3 The result of a new equipment and adiabatic temperature rise test [1]

2.1.2 Thermal conductivity

Temperature distribution in concrete structures depends on thermal conductivity of concrete. It is widely accepted that it is important to use appropriate model of thermal conductivity for temperature distribution analysis. Thermal conductivity of concrete is affected by mix proportion of concrete, type and content of aggregate, relative humidity of concrete and temperature.

Experiments were conducted to develop a new thermal conductivity model [2]. QTM-D3 device was used to calculate thermal conductivity of concrete. The result of the experiments are shown in Fig. 4.

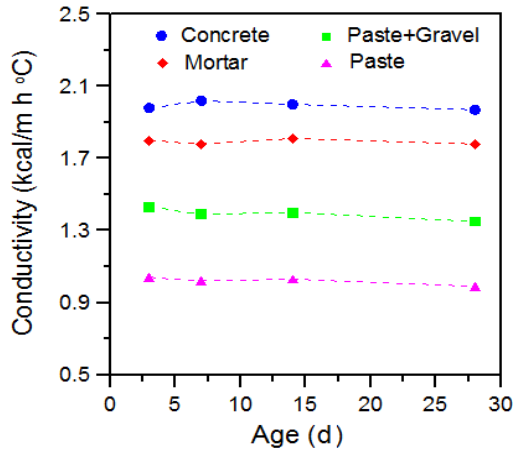

(a) Age

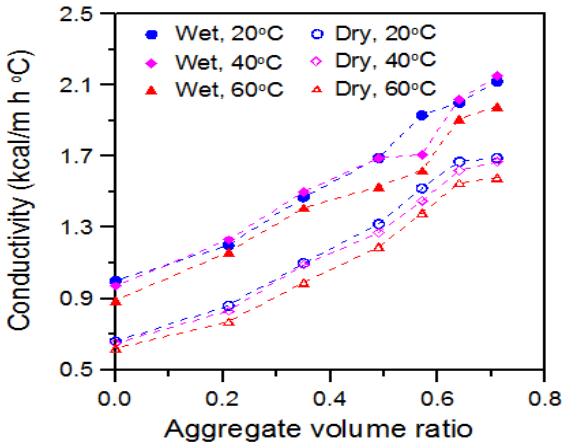

(b) Aggregate content

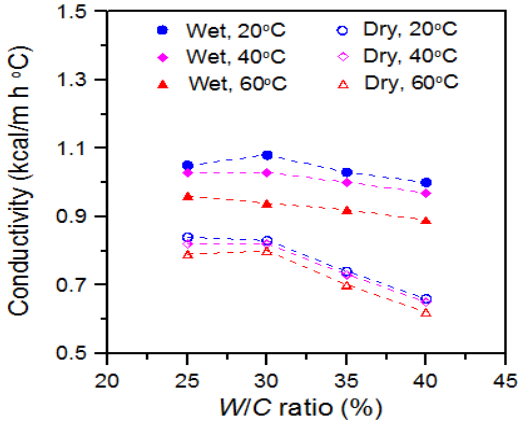

(c) W/C ratio of paste

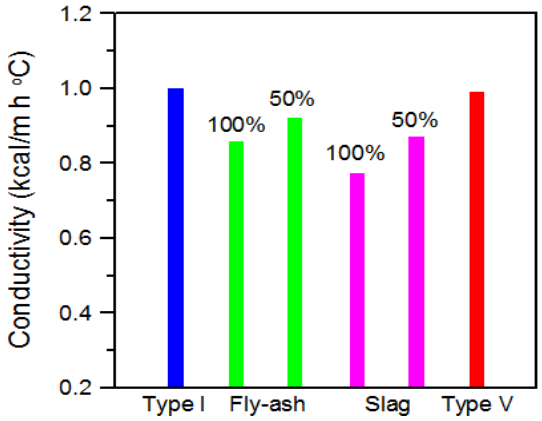

(d) Type of cementitious materials

Fig. 4 Experimental result of thermal conductivity [2]

Using the result of the experiments, a prediction model has been developed as Eq. (2). Fig. 5 shows a close relationship between the value obtained from the developed model and measured value by experiments.

$$k_c = k_{ref}[0.293 + 1.01AG] \times [0.8(1.62 - 1.54(W/C)) + 0.2R_h] \times [1.05 - 0.0025T] \times [0.86 + 0.0036(S/A)] \quad (2)$$

where, k_c is conductivity of concrete(kcal/m·h·℃), k_{ref} is conductivity measured at a condition of $AG = 70$, $W/C = 0.4$, $S/A = 0.4$, $T = 20$, AG is aggregate ratio, W/C is water-cement ratio, R_h is relative humidity of concrete, T is temperature of concrete(℃) and S/A is fine aggregate volume fraction.

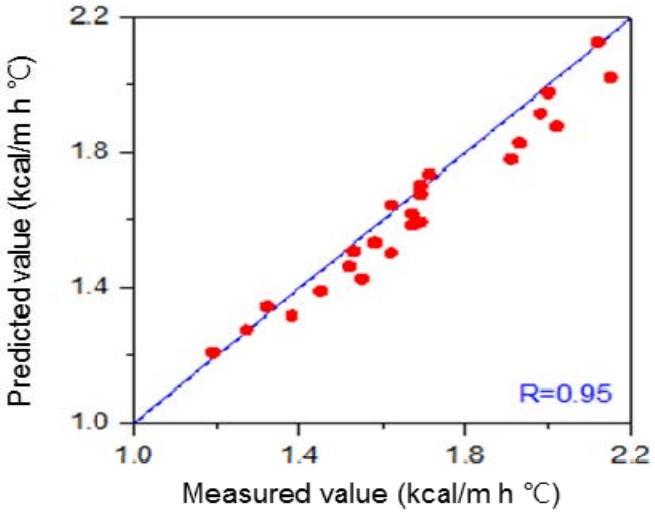

Fig. 5 Comparison of the measured and predicted values [2]

2.1.3 Convective heat transfer coefficient

Convective heat transfer coefficient, which is one of the most important thermal factors, represents heat transfer between concrete surface and ambient air.

Therefore, temperature gradient in concrete members is affected convective heat transfer coefficient and thermal conductivity.

Experiments were conducted to develop convective heat transfer coefficient model and an overview of the experiment's set-up is shown in Fig. 6 [3]. Each experiment on several wind velocities was performed for different kinds of cuing conditions, which are exposure, steel and wood form with thickness 10mm and 20mm.

The result of the experiments is shown in Fig. 7. As shown in Fig. 7, temperature distribution of specimen is different with wind velocity and type of formwork. Using the result of the experiments, a prediction model has been developed as Eq. (3). Fig. 8 shows a close relationship between the calculated value by the developed model and measured value.

$$\overline{H}_c = \frac{1}{\left\{\frac{L_f}{\alpha k_f} + \frac{1}{14.5 + 4.11\nu^{4/5}L^{-1/5}}\right\}} \tag{3}$$

where, $\overline{H}_c$ is convective heat transfer coefficient(kcal/h·m^2·℃), L_f is depth of formwork(m), α is conductivity(kcal/h·m·℃), ν is wind velocity(m/s) and L is convective length(m).

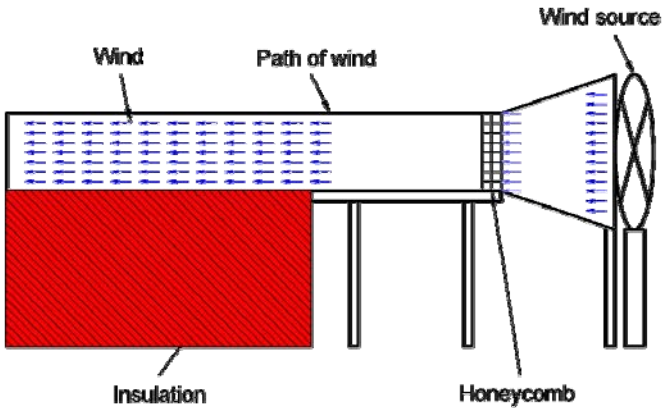

Fig. 6 An overview of the experiment's set-up for convective heat transfer [3]

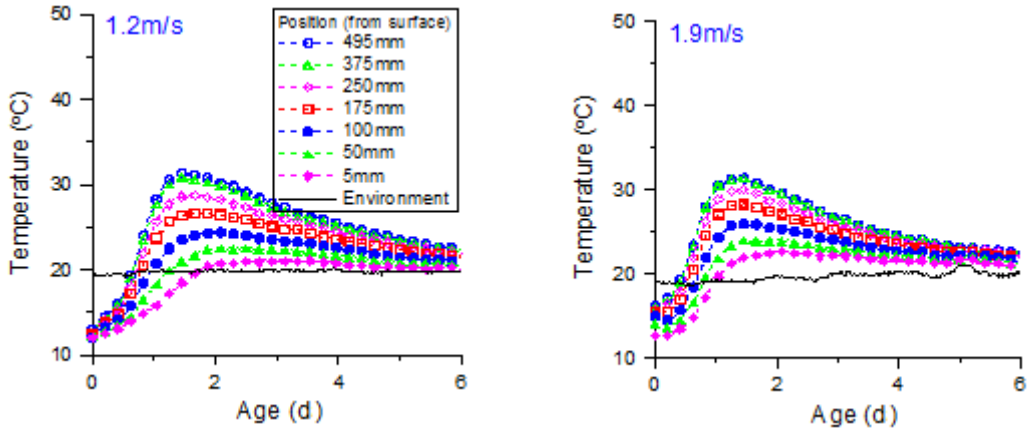

(a) Variation with wind velocity

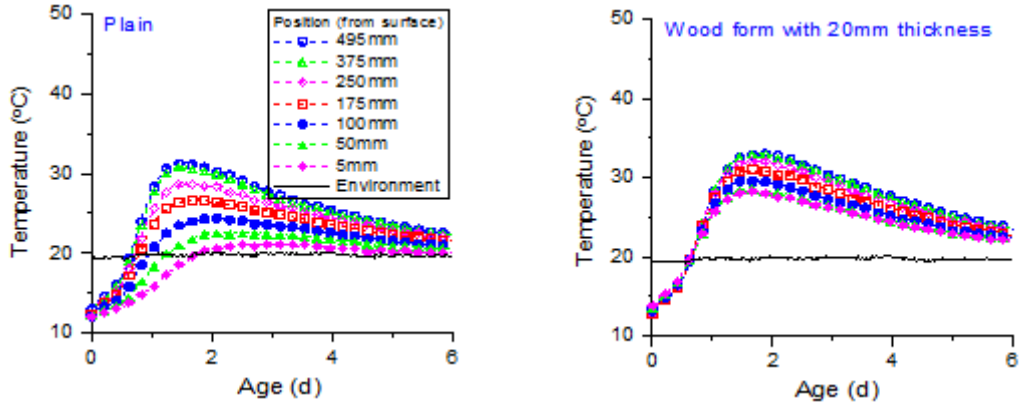

(b) Variation with type of formwork

Fig. 7 The result of experiments for convective heat transfer [3]

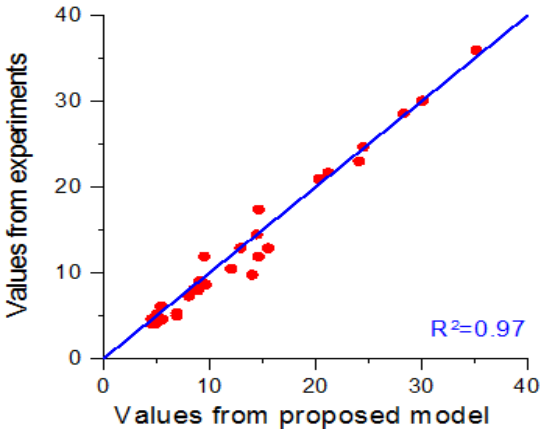

Fig. 8 Comparison of the measured and predicted value [3]

2.1.4 Mechanical properties of concrete

Thermal stress and possibility of cracks are greatly affected by mechanical properties of concrete, such as compressive strength, tensile strength and elastic modulus. Therefore, it is necessary to develop appropriate prediction model. When mechanical properties of concrete is calculated, the effect of temperature should be included because a rise in the curing temperature speeds up the chemical reactions of hydration and thus affects the strength of concrete.

(1) Compressive strength

The influence of heat of hydration on strength has emphasized the importance of estimating the strength development of concrete as a function of temperature and age. Maturity is usually used to apply the effect of temperature and age to strength of concrete [5-7]. Freiesleben Hansen and Pedersen proposed the Arrhenius function. However, Arrhenius function overestimated the effect of temperature at later age [5]. To overcome the shortcoming of Arrhenius function, compressive strength was suggested as Eq. (4) by using apparent activation energy which is a function of age [9].

$$\frac{S}{S_u} = \left[1 - \frac{1}{\sqrt{1 + A\sum_{i=1}^{n} \left(e^{-\frac{E_0}{RT} e^{-\alpha t_i}} + e^{-\frac{E_0}{RT} e^{-\alpha t_{i-1}}} \right) (t_i - t_{i-1})}} \right] \tag{4}$$

where, S is compressive strength(MPa), S_u is limiting compressive strength(MPa), t is age(day), T is curing temperature(℃), R is gas constant(J/K·mol), α, A are constant, E_0 is initial apparent activation energy(J/mol) and t_0 is age when strength development starts(day).

Fig. 9 shows the relative compressive strength estimated from various models compared with the experimental relative strength. Eq. (4) can estimate the compressive strength with curing temperature and age accurately.

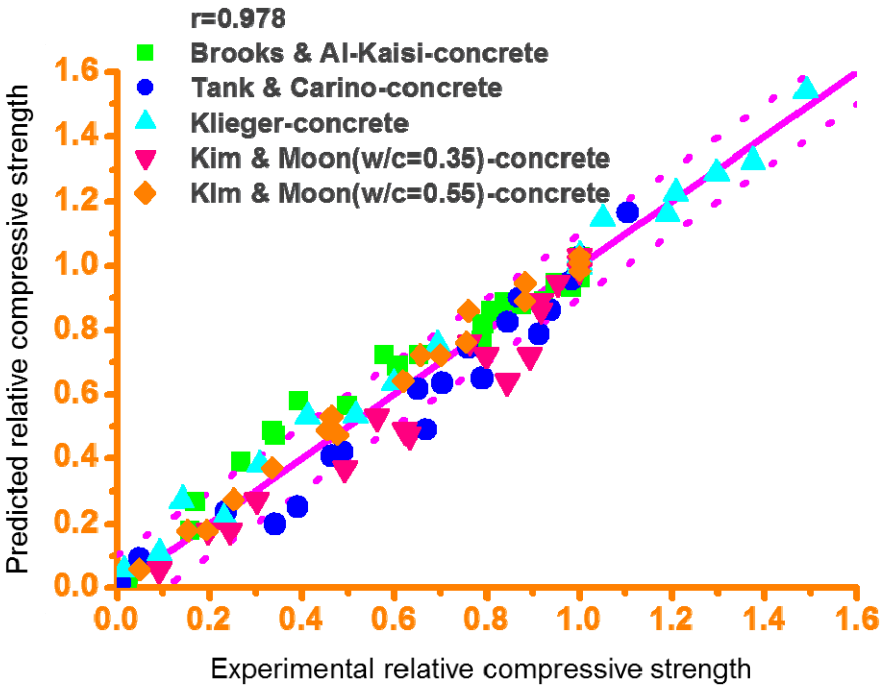

Fig. 9 Comparison with other researches [9]

(2) Splitting tensile strength and elastic modulus

Splitting tensile strength and elastic modulus can be expressed as a function of compressive strength [10]. Based on compressive strength development obtained Eq. (4), splitting tensile strength and elastic modulus were proposed as Eq. (5) and Eq. (6) respectively [11].

$$f_{sp} = 0.31 f_{cu}^{0.71} \tag{5}$$

where, f_{sp} is splitting tensile strength(MPa) and f_{cu} is compressive strength(MPa).

$$E_c = 5{,}250 f_{cu}^{0.46} \tag{6}$$

where, E_c is elastic modulus(GPa) and f_{cu} is compressive strength(GPa).

Fig. 10 and Fig. 11 show splitting tensile strength and elastic modulus estimated from various models compared with the experiment result. Eq. (5) and Eq. (6) can accurately estimate splitting tensile strength and elastic modulus with curing temperature and age respectively.

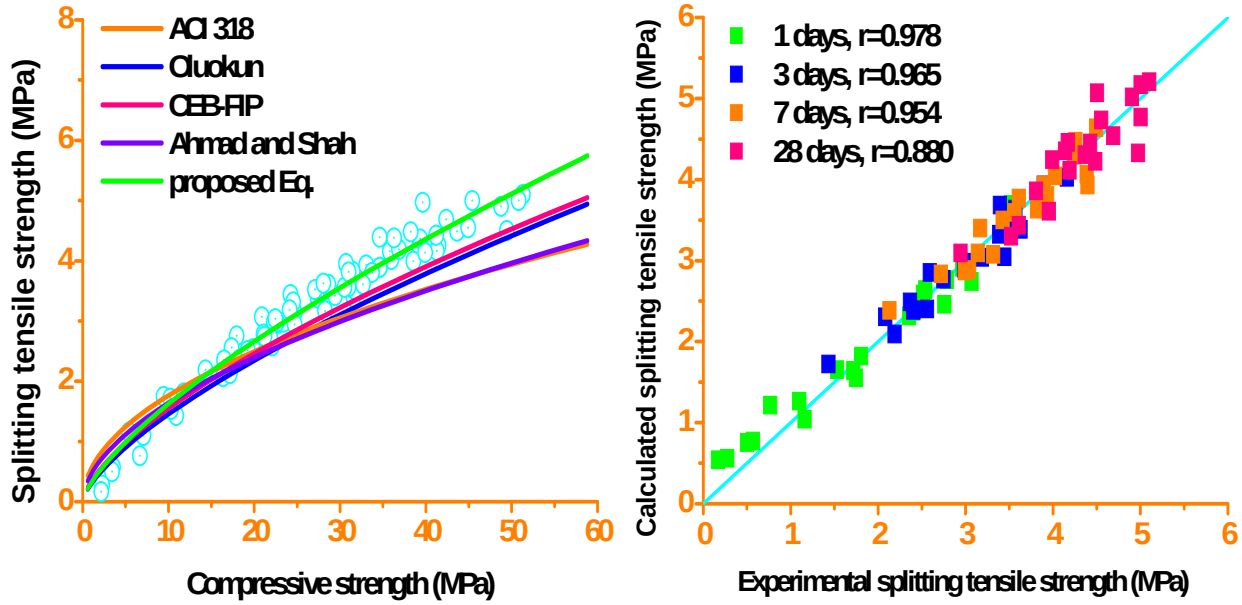

(a) Relation between compressive strength and splitting tensile strength

(b) Comparison of model equation and experiment result

Fig. 10 Comparison various splitting tensile strength models with experiment result [11]

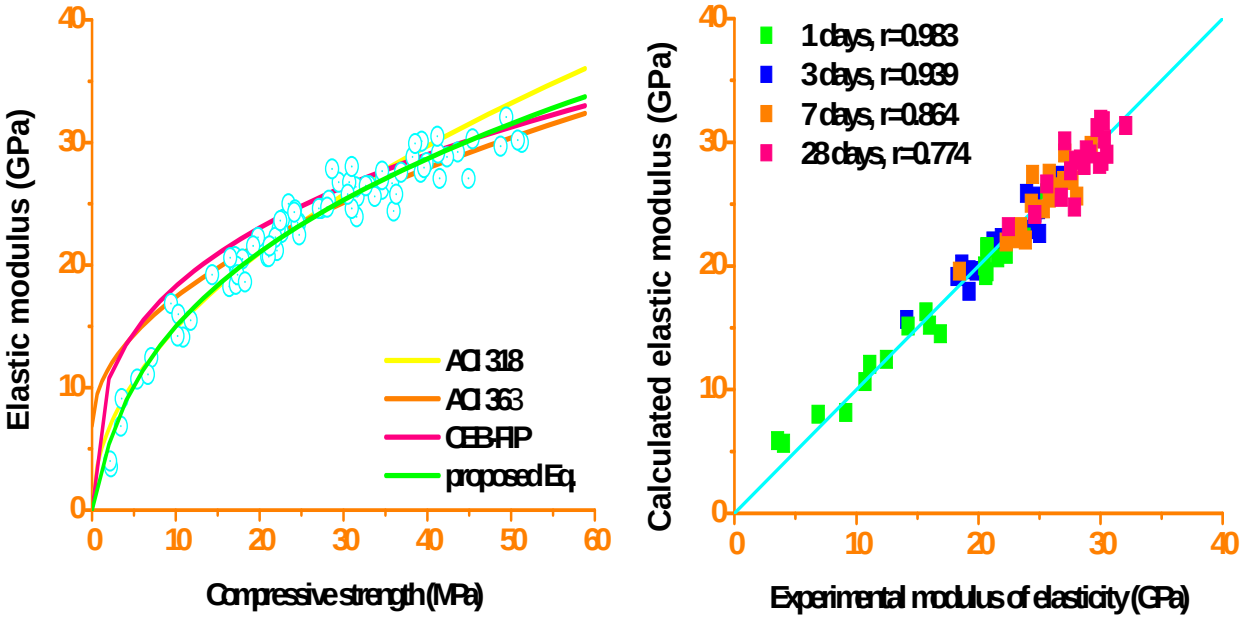

(a) Relation between compressive strength and elastic modulus

(b) Comparison of model equation and experiment result

Fig. 11 Comparison various elastic modulus models with experiment result [11]

2.2 Development of analysis program

2.2.1 Finite element formulation

(1) Heat transfer

Thermal conduction in concrete is governed by Fourier's law, which is given by Eq. (7) and boundary condition is given by Eq. (8). As shown in Eq. (7) and Eq. (8), heat transfer in concrete depends on thermal conductivity, specific heat and convective heat transfer coefficient.

$$\rho c \frac{\partial T}{\partial t} = k\left[\frac{\partial^2 T}{\partial x^2} + \frac{\partial^2 T}{\partial y^2} + \frac{\partial^2 T}{\partial z^2}\right] + q^B \tag{7}$$

where, ρ is density, c is specific heat, T is temperature, t is time and q^B is the rate of thermal energy generated per unit volume.

$$k\left[\frac{\partial T}{\partial x} n_x + \frac{\partial T}{\partial y} n_y + \frac{\partial T}{\partial z} n_z\right] + q_c = 0 \tag{8}$$

where, k is thermal conductivity, n is vector perpendicular to the direction of heat transfer and q_c is the heat transfer rate per unit area.

If the temperature in concrete at time t (=$T(x, y, z, t)$) is expressed as a product of shape function (=$N(x, y, z)$) and the temperature at the FE nodes at time t is expressed as {$temp(t)$}, and then the Galerkin's method is applied to Eq. (7) and Eq. (8), Eq. (9) is obtained.

$$[k]\{temp(t)\} + [c]\left\{\frac{\partial temp(t)}{\partial t}\right\} = \{q\} \tag{9}$$

where,
$$[k] = \int_{V_e} k\left(\frac{\partial [N]^T}{\partial x}\frac{\partial [N]}{\partial x} + \frac{\partial [N]^T}{\partial y}\frac{\partial [N]}{\partial y} + \frac{\partial [N]^T}{\partial z}\frac{\partial [N]}{\partial z}\right) dV$$

$$[c] = \int_{V_e} [N]^T [N] \rho c dV$$

$$\{q\} = \int_{S_e} k[N]^T \frac{\partial T}{\partial n} dS + \int_{V_e} q^B [N]^T dV$$

In the numerical formulation of $\{q\}$, boundary conditions are defined as Eq. (10) for exposed surface of concrete, S.

$$k\left(\frac{\partial T}{\partial n}\right)_{at\ S} = h_c(T_{air} - T_s) \tag{10}$$

where, k is thermal conductivity, h_c is convective heat transfer coefficient, T_S is temperature of concrete surface, and T_{air} is ambient temperature.

Using Eq. (10), $[k]$ and $\{q\}$ can be expressed as follow.

$$[k] = \int_{V_e} k\left(\frac{\partial [N]^T}{\partial x}\frac{\partial [N]}{\partial x} + \frac{\partial [N]^T}{\partial y}\frac{\partial [N]}{\partial y} + \frac{\partial [N]^T}{\partial z}\frac{\partial [N]}{\partial z} \right) dV + \int_{S_e} h_c [N]^T T_s dS \qquad (11a)$$

$$\{q\} = \int_{S_e} h_c [N]^T T_{air} dS + \int_{V_e} q^B [N]^T dV \qquad (11b)$$

The general FE equation for entire structures can be expressed as Eq. (12).

$$[K]\{T\} + [C]\{\frac{\partial T}{\partial t}\} = \{Q\} \qquad (12)$$

where, $\{T\} = \sum_e \{temp(t)\}$, $[K] = \sum_e [k]$, $[C] = \sum_e [c]$, $\{Q\} = \sum_e \{q\}$

(2) Stress

Using minimum potential energy principle, the general FE equation for stress is given by Eq. (13) and Eq. (14). This equation considers creep, thermal stress and shrinkage stress.

$$\frac{\partial \pi}{\partial \{d\}} = \left\{ \int_V [B]^T [D]\,[B] dV \right\} \{d\} - \int_V [B]^T [D][\{\varepsilon_c\} + \{\varepsilon_T\} + \{\varepsilon_{sh}\}] dV - \{F\} = 0 \qquad (13)$$

$$[K]\{d\} = \{F\} + \{F\}_c + \{F\}_T + \{F\}_{sh} \qquad (14)$$

where, $[K] = \int_V [B]^T [D]\,[B] dV$: Stiffness matrix

$\{F\}_c = \int_V [B]^T [D] \{\varepsilon\}_c dV$: Creep

$\{F\}_T = \int_V [B]^T [D] \{\varepsilon\}_T dV$: Temperature

$\{F\}_{sh} = \int_V [B]^T [D] \{\varepsilon\}_{sh} dV$: Shrinkage

2.2.2 Developed program(CONSA/HS)

Using above mentioned models and equations, analysis program for temperature distribution and thermal stress has been developed by KAIST concrete lab., which name is CONSA/HS(CONcrete Stress Analyzer/Hydration and Shrinkage).

(1) Pre-processor

Pre-process of CONSA/SH can be connected with MIDAS GEN/CIVIL. As shown in Fig. 12, Mesh file from MIDAS can be converted to that of CONSA/SH.

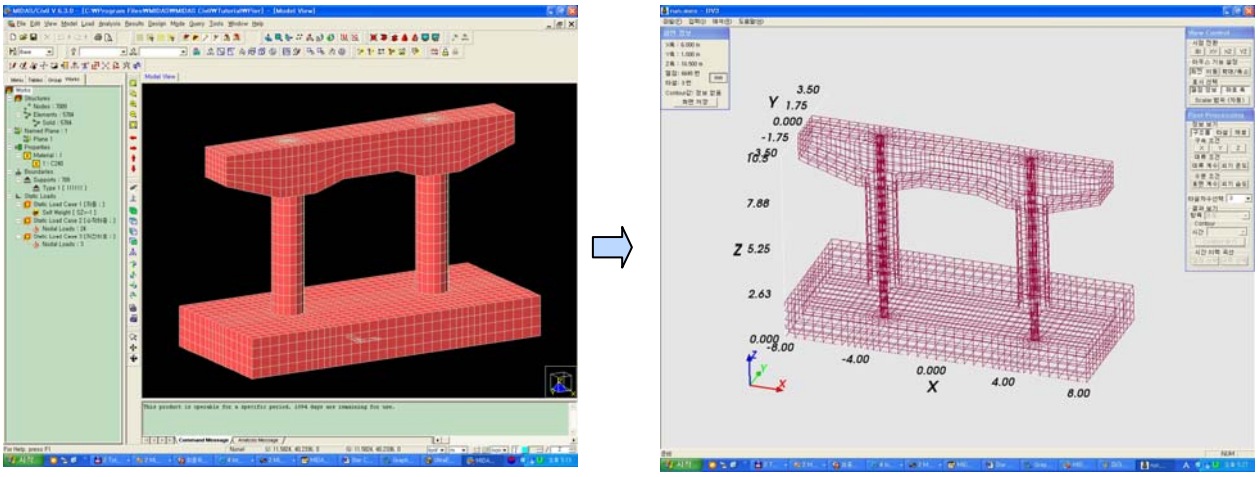

(a) MIDAS (b) CONSA/HS

Fig. 12 Pre-process

(2) Main solver

CONSA/SH can consider various effects. Detailed features are shown in Table 1.

Table 1 Features of CONSA/HS

Features

3D structures analysis
Application of pipe-cooling effect
Application of creep effect
Application of mechanical property development
Application of placement stage
Application of environmental conditions
Correlation of hydration and shrinkage

(3) Post-processor

As shown in Fig. 13, CONSA/SH provides various post-process such as temperature distribution, stress distribution, crack index and history of temperature, stress and crack index.

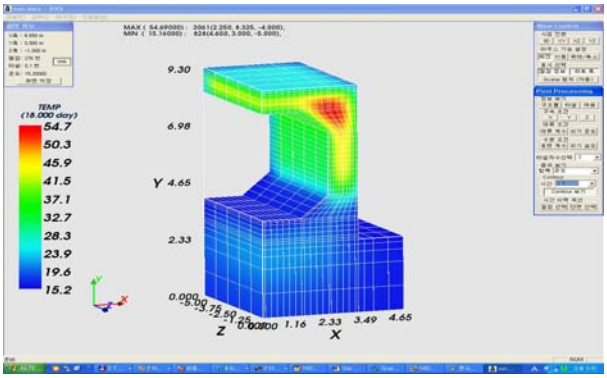

(a) Temperature

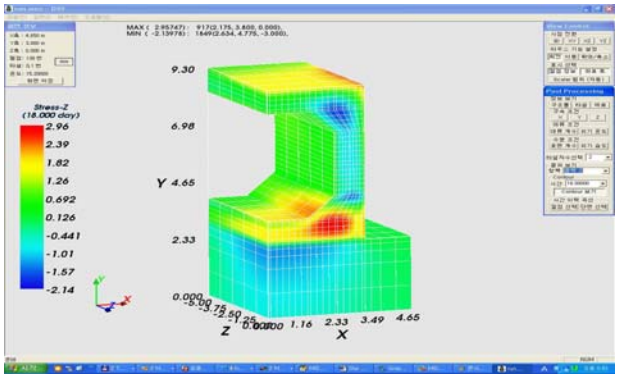

(b) Stress

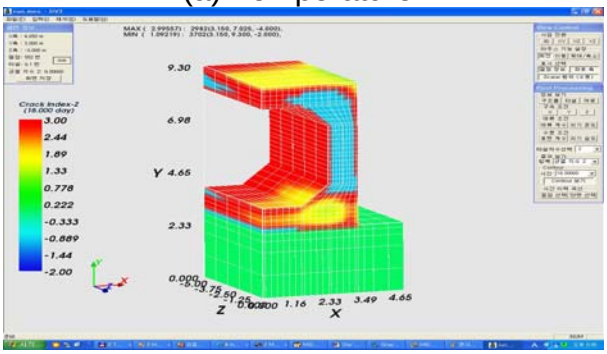

(c) Crack index

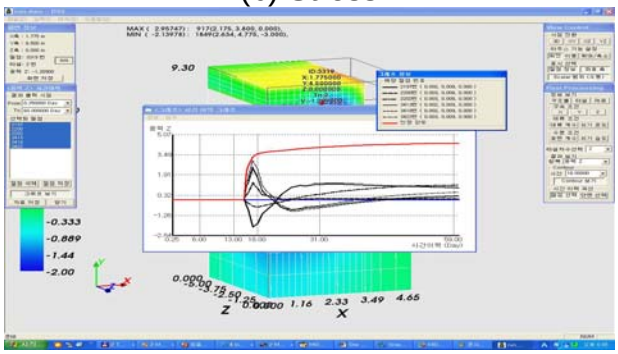

(d) History of temp., stress and crack index

Fig. 13 Post-process

2.3 Application for concrete structures

CONSA/HS has been used in real structures which are foundation of bridges, Dams, Nuclear power plant, subway structures and buildings. In this paper, the result of application for Seongdeok Dam is presented.

Seongdeok Dam, which is located in Kyung-Ju, is analyzed for temperature and thermal stress distribution. The shape of Seongdeok Dam is shown in Fig. 14 and input parameters are given in Table 2.

The result of analysis is shown in Fig. 15 and Fig. 16. Fig. 16 shows the temperature and stress history at center and surface of dam. Temperature of the dam rises rapidly to the highest temperature and then falls down slowly. Thermal stress is compressive at early age and converts into tension as the age of concrete increases.

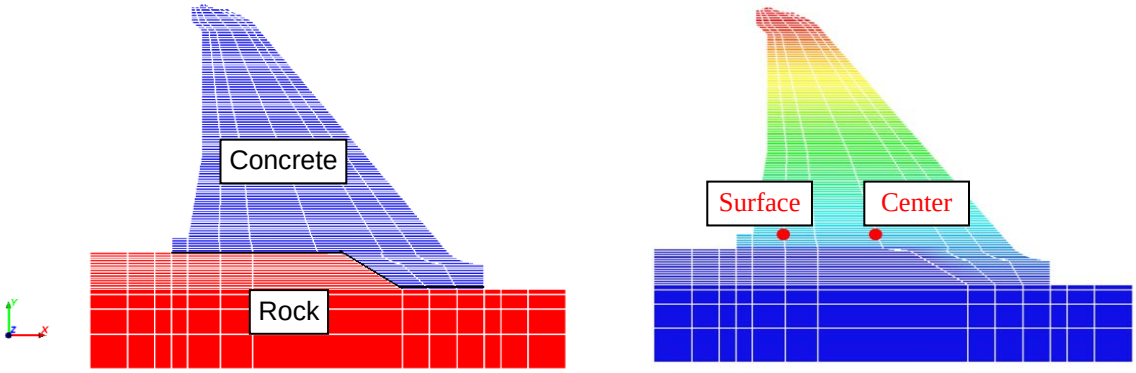

Fig. 14 The shape of Seongdeok Dam

Table 2 Input parameters for Seongdeok dam analysis

Parameters		Value
Adiabatic temperature rise	Maximum temperature rise(℃)	30.1
	Rate of reaction	0.477
Thermal properties	Thermal conductivity(kcal/m·h·℃)	2.3
	Specific heat(kcal/kg·℃)	0.25
	Convective heat transfer coefficient(kcal/m^2·h·℃)	12
	Unit density(kg/m^3)	2400
	Thermal expansion coefficient(/℃)	$10X10^{-6}$
Material properties	Compressive strength(MPa)	12
	Elastic modulus(GPa)	-
	Poisson's ratio	0.18

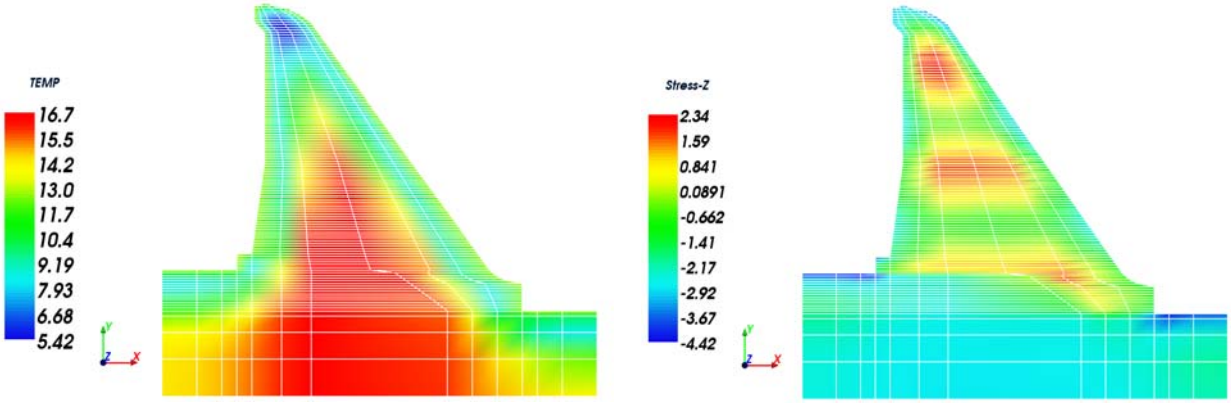

(a) Temperature distribution (b) z-dir. Stress distribution

Fig. 15 The result of the analysis for Seongdeok Dam (age : 5 year)

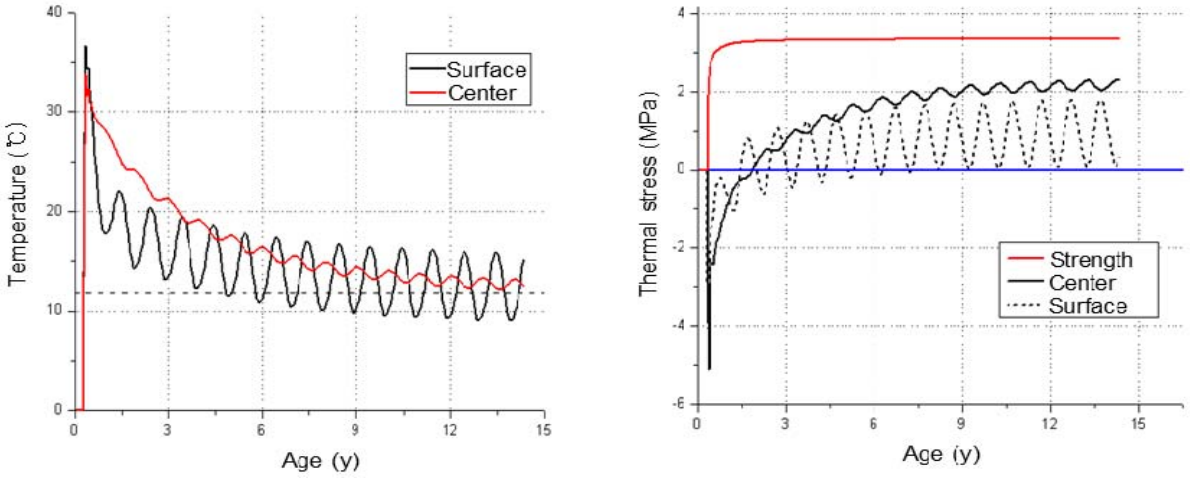

(a) Temperature (b) Stress

Fig. 16 Temperature and stress history

3. PREDICTION OF THERMAL STRESS USING AN EXPERIMENTAL DEVICE

3.1 Experimental device for measuring thermal stress

For numerical analysis, there is difficulty of calculating accurate properties of concrete at early age. To overcome this difficulty, an experimental device has been developed. As compared in Fig. 1 and Fig. 17, lots of uncertainties can be ignored such as elastic modulus, creep and thermal expansion coefficient etc. because this device measures thermal stress by product of the strain and the elastic modulus of constraint material directly.

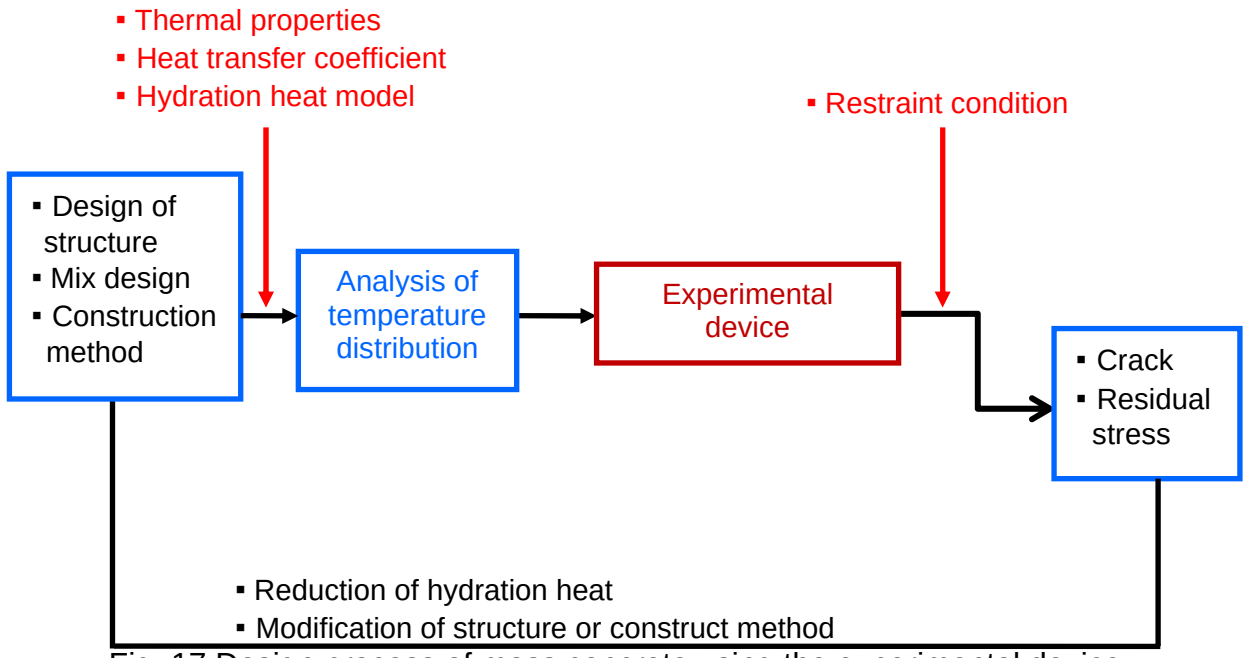

Fig. 17 Design process of mass concrete using the experimental device

3.1.1 Concept of the experimental device

The concept and shape of an experimental device are shown in Fig. 18 and Fig. 19 [12]. It is important to use constraint material, which has different thermal expansion coefficient from concrete, because different expansion between constraint material and concrete under same temperature history induces thermal stress. More specifically, when constraint material with lower thermal expansion coefficient than that of concrete is used, the device simulates thermal stress at interior of structures due to internal restraint or thermal stress at whole section due to external restraint. However, when constraint material with higher thermal expansion coefficient than that of concrete is used, the device simulates thermal stress at surface of structures due to internal restraint. This device also uses 3 different thickness constraint materials to simulate the amount of restraint, which influences on thermal stress.

Under equilibrium condition between constraint material and concrete, the force of concrete is the same amount of the force of the constraint material. Stress of concrete can be calculated using Eq. (15)

$$\sigma_c = \frac{F_c}{E_c A_c} = \frac{F_f}{E_c A_c} = \frac{E_f \varepsilon_f A_f}{E_c A_c} \tag{15}$$

where, σ is stress, F is force, E is elastic modulus, A is area, ε is strain and c and f represent concrete and constraint material respectively.

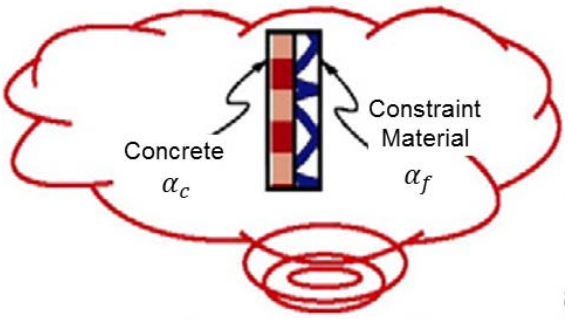

(a) Prescribed condition

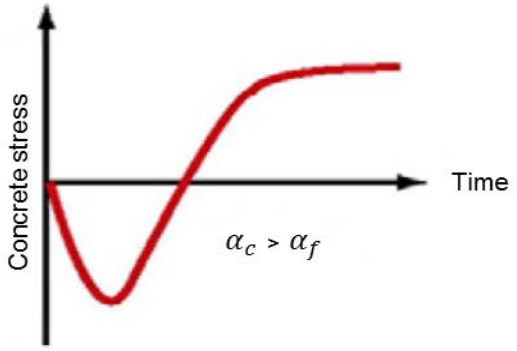

(b) Internal (interior) and external restrain

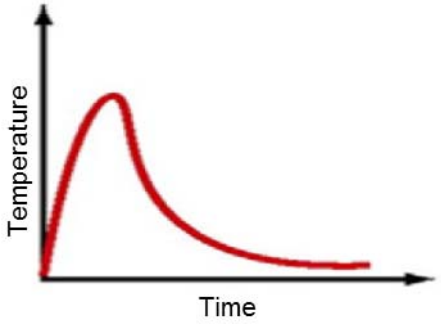

(c) Temperature of concrete

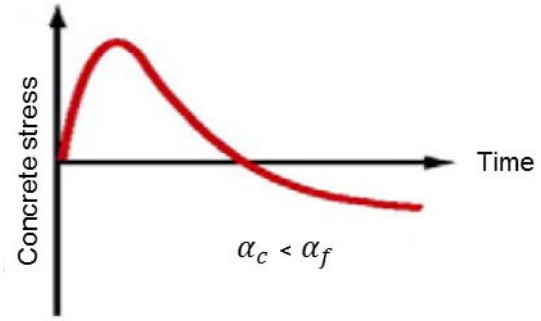

(d) Internal restraint (surface)

Fig. 18 Concept of the experimental device [12]

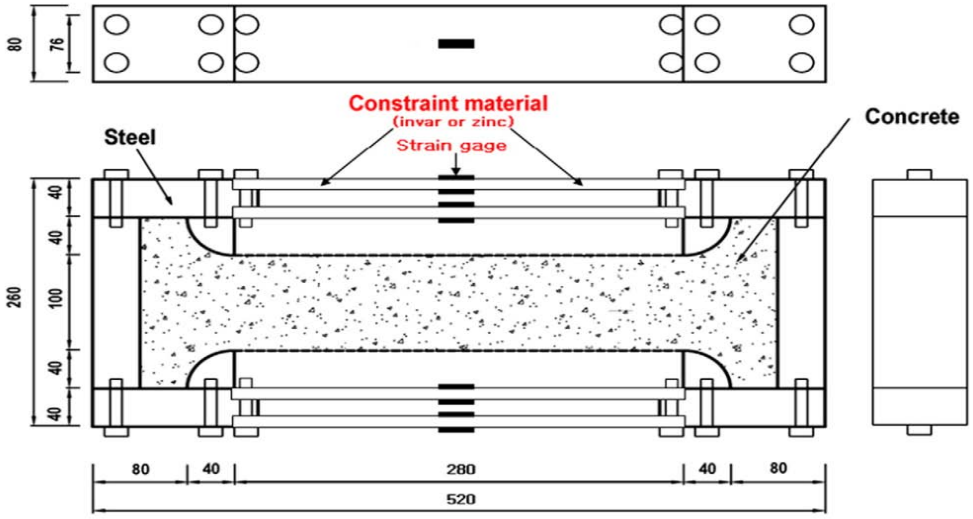

Fig. 19 Shape and dimensions of the experimental device [12]

3.1.2 Experimental procedure

Before the experiment, the temperature and humidity values for the chamber was inserted from the temperature history calculated using an analysis program. To reduce drying shrinkage, humidity is kept over 85%. Eight strain gages are used for measuring the strain of the constraint material. An overview of the experimental procedure is shown in Fig. 20.

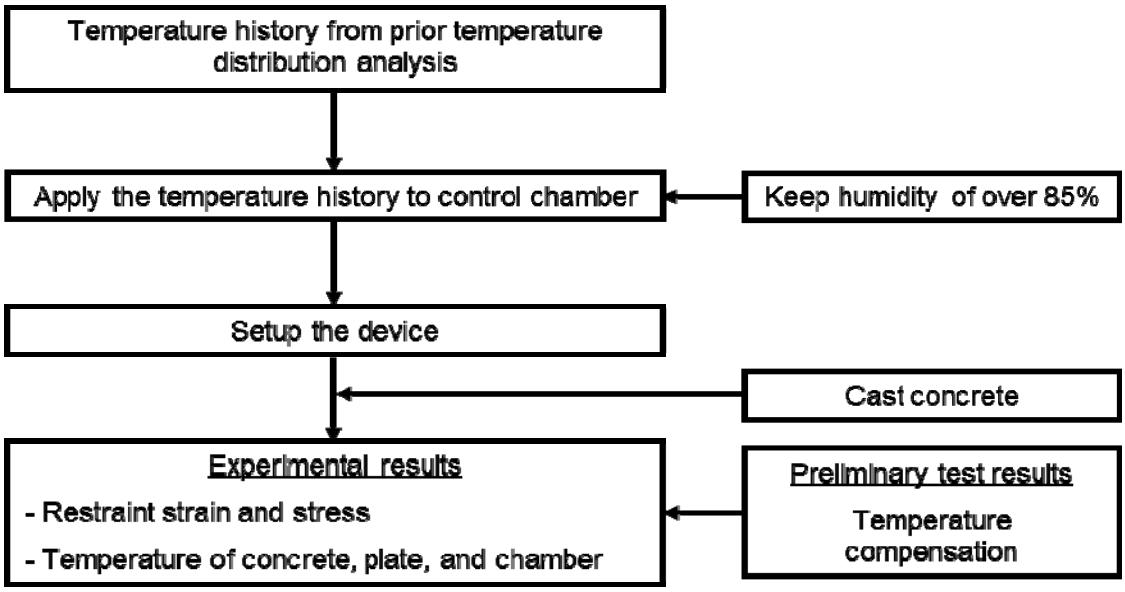

Fig. 20 Experimental procedure

3.1.3 Experiment result

Mix proportion of concrete and Material properties of constraint materials are shown in Table 3 and Table 4 respectively.

Table 3 Mix proportion of concrete

W/C	S/a (%)	Unit (kg/m^3)					
		W	C	S	G	Admixture	
						AE	WR
0.4	39	160	400	726	989	0.02	0.2

Table 4 Material properties of constraint materials

Material	Thickness (mm)	Thermal expansion coefficient (X 10^{-6}/℃)	Elastic modulus (GPa)	Type of restraint
Invar	10, 20, 40	1.5	28.3	External
Zinc	10, 20, 40	25	108	Internal

Fig. 19 shows the result of experiment. As shown in Fig. 21, amplitude of stress increases by increasing the restraining force and stress due to hydration and restraint is simulated even though properties of concrete at early age are uncertain.

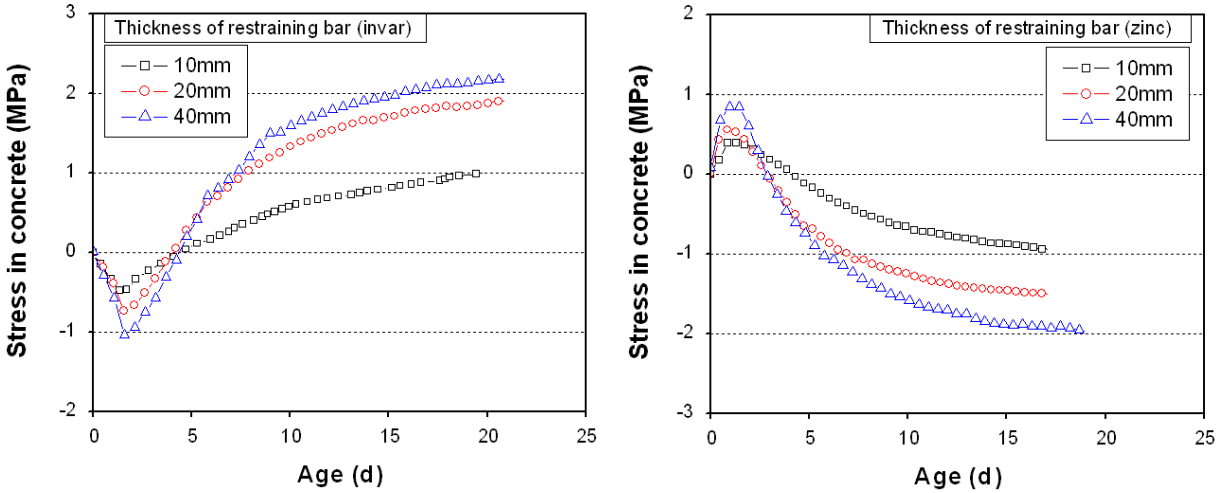

(a) Invar (b) Zinc

Fig. 21 The result of experiment [12]

3.2 Application of an experimental device for measuring thermal stress

3.2.1 Application method

Once Restraint strain (which is the difference between stress independent strain and total strain) and restraint stress are measured by experimental device, a relation between restraint strain and restraint stress can be developed with respect to degree of restraint and age. Consequently, if degree of restraint in concrete structures are calculated, thermal stress can be calculated by using the relation.

3.2.2 Application in field

The experimental device was applied to Seongdeok Dam, which is located in Kyung-Ju, Korea [13]. To verify the results, temperature history, total strain and stress were measured in field. Fig. 22 shows an overview of the construction site.

Fig. 23 shows comparison of the temperature history obtained from construction site and analysis, where the temperature distribution analysis shows a good prediction compared the construction site.

Fig. 24 shows the results of experiments, which are stress-independent strain, total strain, restraint strain and restraint stress.

Using the results, thermal stress in the structure can be calculated. The relation between restraint strain and stress is shown in Fig. 25. In this case, restraint strain of the structure are 50.62 at 5 day and 32.43 at 25 day. According to the relation, stresses are 18.58 MPa at 5 day and 3.66 MPa at 25 day.

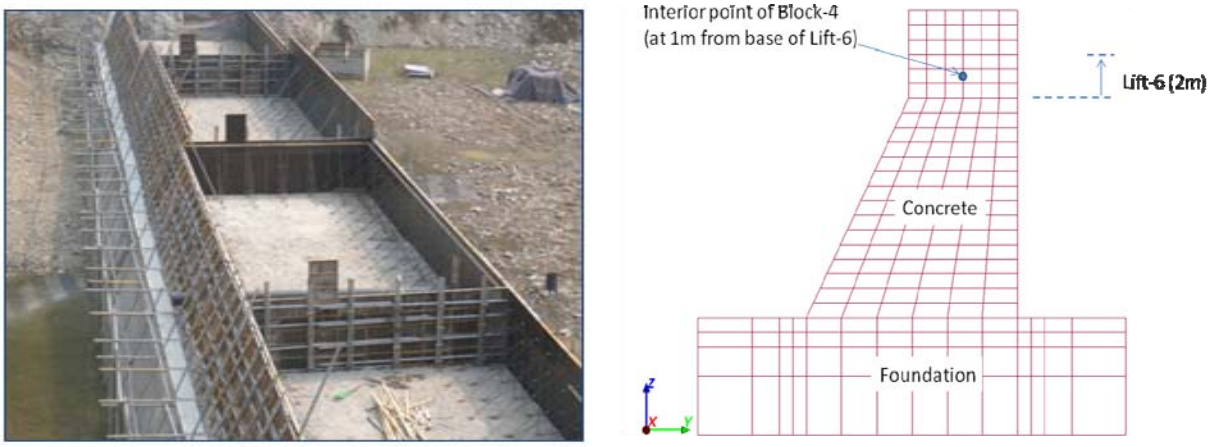

Fig. 22 An overview of construction site [13]

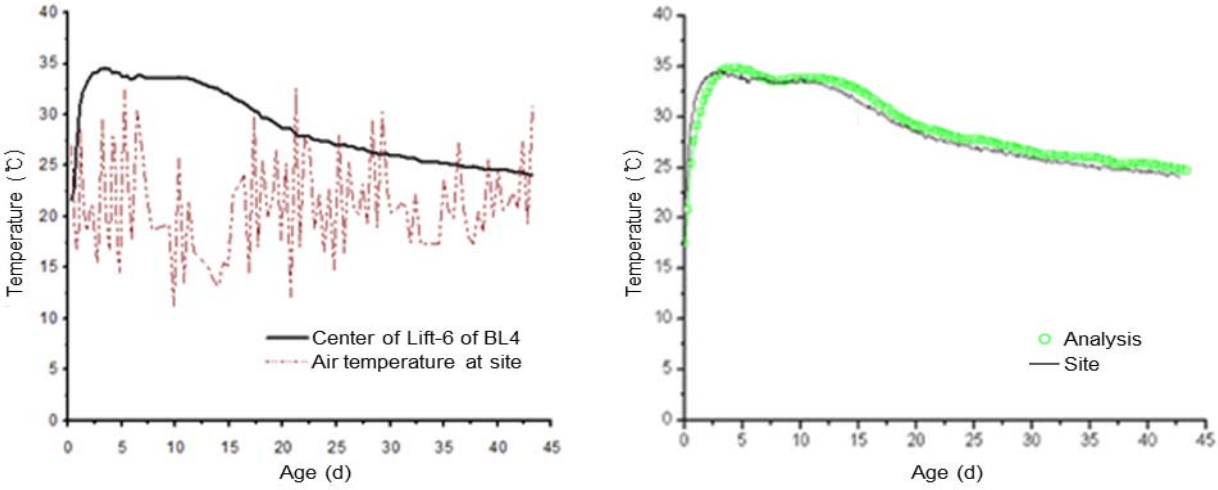

Fig. 23 Measured temperature from field and analysis result [13]

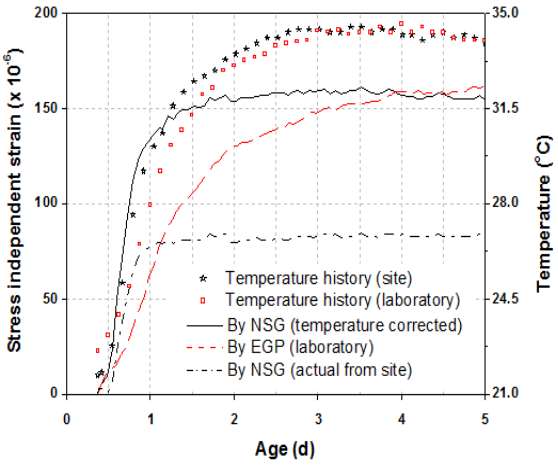

(a) Stress-independent strain

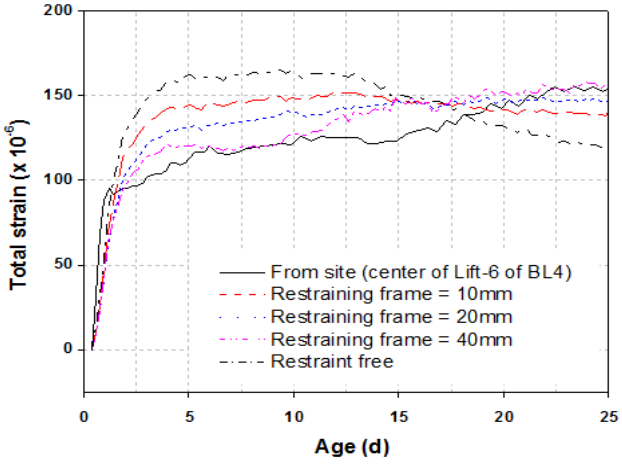

(b) Total strain

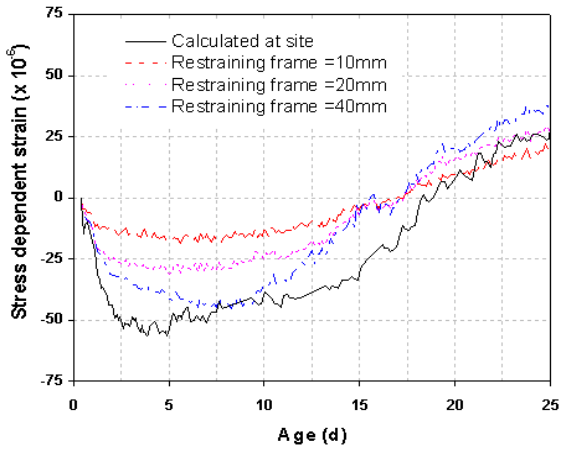

(c) Restraint strain

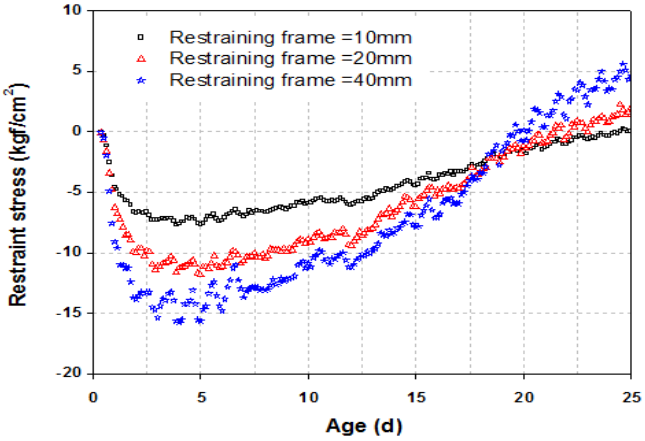

(d) Restraint stress

Fig. 24 Experiment result [13]

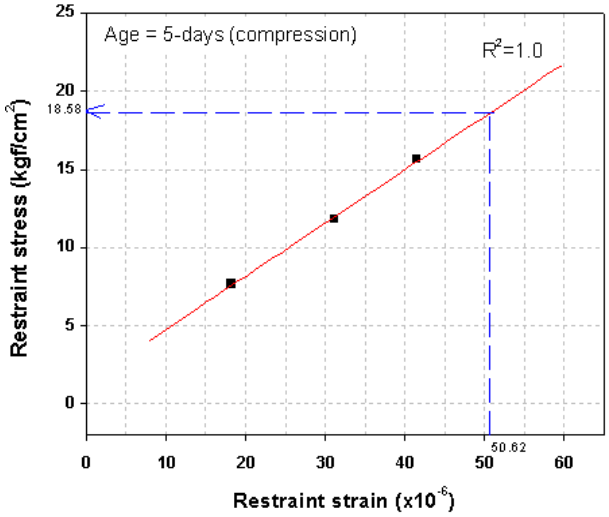

(a) 5 day

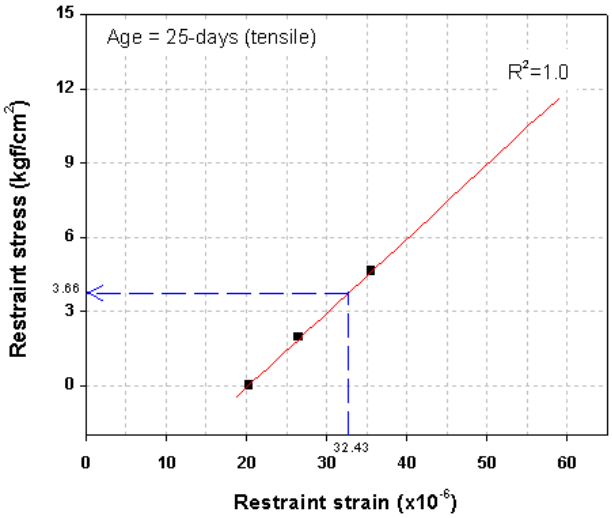

(b) 25 day

Fig. 25 Relation between restraint strain and stress [13]

3.2.3 Limitation of application

As shown in Fig. 26, the amount of restraint is different between external restraint, which falls down continuously, and internal restraint, which rises rapidly to the highest restraint and then falls down slowly. However, developed device can reproduce only external restraint. Therefore, there is a limitation of application for structures that have strong internal restraint. To overcome this limitation, two approaches are suggested.

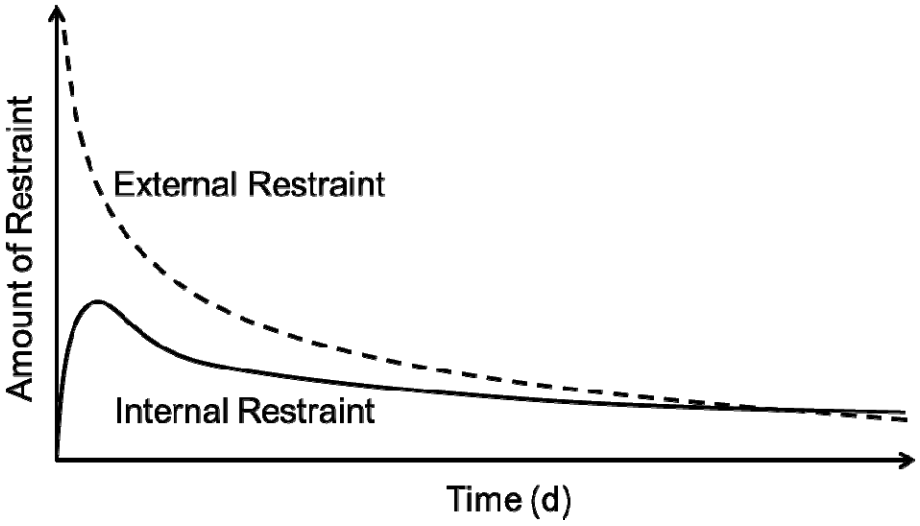

Fig. 26 External restraint and internal restraint

(1) Calculating the uncertainties of concrete using the experimental device

When numerical analysis for thermal stress are performed, there is difficulty of defining uncertainties of concrete, such as creep coefficient, elastic modulus, thermal expansion coefficient and shrinkage. If the uncertainties are accurately defined, the result of numerical analysis will have reliability.

The uncertainties can be obtained by comparing the experiment result with numerical analysis of the experimental device. Each step has the best values of the uncertainties that would result in similar stress result between numerical analysis and experiment. Using regression analysis, uncertainties can be expressed as a function of time and can be used for analyzing structures.

(2) Defining the correct factor

Thermal stress depends on type of restraint and geometry of structures and total thermal stress can be divided into the stress induced by internal restraint and external restraint. Therefore, if structures are categorized according to the type of restraint and geometry such as the ratio of height to length, correct factor can be defined. For example, there is wall which has the 70% effect of external restraint and the 30% effect of internal restraint. The stress due to external restraint can be calculated by using experimental result directly and the stress due to internal restraint and geometry can be calculated as the product of the stress and correct factor.

4. CONCLUSION

In this paper, two different types of approaches for predicting the thermal stress induced by hydration heat are overviewed. Although both approaches successfully simulated thermal stress in concrete structures, they still have limitation and difficulty in specific conditions. Therefore, more research should be performed to predict more accurate thermal stress.

ACKNOWLEDGMENTS

This work (20111520100090) was supported by the Nuclear Research & Development of the Korea Institute of Energy Technology Evaluation and Planning (KETEP) grant funded by the Korea government Ministry of Knowledge Economy. The authors wish to express their gratitude for the financial support that has made this study possible.

REFERENCES

[1] E. W. Jin (2012), "Development of Equipment for Measuring Adiabatic Temperature Rise of Concrete by Compensating Heat Loss", *M.S. Thesis, Korea Advanced Institute of Science and Technology*, 36, 50 and 51 pages

[2] K. H. Kim, S. E. Jeon, J. K. Kim and S. C. Yang (2003), "An experimental study on thermal conductivity of concrete", *Cement and Concrete Research*, 33 (2003) 363-371

[3] S. E. Jeon and J. K. Kim (2003), "Experimental Study on Coefficient of Air Convection" *Journal of the Korea Concrete Institute*, Vol.15, No.2, pp.305-313

[4] Y. Lee, M. S. Choi, S. T. Yi and J. K. Kim (2009), "Experimental study on the convective heat transfer coefficient of early-age concrete" *Cement and Concrete Composites*, 31 (2009) 60-71

[5] P. Freiesleben Hansen, E.J. Pedersen (1977), "Maturity computer for controlled curing and hardening of concrete", *Nord. Betong,* 1 (1977) 21-25

[6] K.M. Alexander, J.H. Taplin (1962), "Concrete strength, cement hydration and the maturity rule", *Aust. J. Appl. Sci.,* 13 (1962) 277–284.

[7] A.G.A. Saul (1951), "Principles underlying the steam curing of concrete at atmospheric pressure", *Mag. Concr. Res*., 2 (6) (1951) 127-140

[8] N.J. Gardner (1990), "Effect of temperature on the early-age properties of Type I, Type III, and Type I/fly ash concrete", *ACI Mater. J.,* 87 (1) (1990) 68-78

[9] J. K. Kim, S. H. Han and K. M. Lee (2001), "Estimation of compressive strength by a new apparent activation energy function" *Cement and Concrete Research*, 31 (2001) 217-225

[10] F.A. Oluokun (1991), Prediction of concrete tensile strength from its compressive strength, ACI Mater. J. 88 (3) (1991) 302–309.

[11] J. K. Kim, S. H. Han and Y. C. Song (2002), "Effect of temperature and aging on the mechanical properties of concrete Part Ⅰ. Experimental result" Cement and Concrete Research, 32 (2002) 1087-1094

[12] M. N. Amin, J. S. Kim, Y. Lee and J. K. Kim (2009), "Simulation of the thermal stress in mass concrete using a thermal stress measuring device" *Cement and Concrete Research*, 39 (2009) 154-164

[13] J. K. Kim, M. N. Amin and I. Y. Chu (2010), "THE APPLICATION OF A STRESS DEVICE FOR THE PREDICTION OF STRESSES DUE TO HYDRATION HEAT IN A DAM STRUCTURE" *Proceedings of the 3rd Asian conference on ecstasy in concrete, ACECON 2010*, pp. 95-112